Anomalous self-energy and fermi surface quasi-splitting in the vicinity of a ferromagnetic instability

A. A. Katanin, Arno P. Kampf, V. Yu. Irkhin

Anomalous self-energy and Fermi surface quasisplitting in the vicinity of a ferromagnetic instability

A. A. Katanin,[1,2] A. P. Kampf,[3] and V. Yu. Irkhin[2]

[1]*Max-Planck-Institut für Festkörperforschung, D-70569 Stuttgart, Germany*

[2]*Institute of Metal Physics, 620219 Ekaterinburg, Russia*

[3]*Institut für Physik, Theoretische Physik III, Elektronische Korrelationen und Magnetismus, Universität Augsburg, D-86135 Augsburg, Germany*

We discuss the low-temperature behavior of the electronic self-energy in the vicinity of a ferromagnetic instability in two dimensions within the two-particle self-consistent approximation, functional renormalization group, and Ward-identity approaches. Although the long-range magnetic order is absent at $T > 0$, the self-energy has a non-Fermi-liquid form at low energies $|\omega| \lesssim \Delta_0$ near the Fermi level, where Δ_0 is the ground-state spin splitting. The spectral function at temperatures $T \lesssim \Delta_0$ has a two-peak structure with finite spectral weight at the Fermi level. The simultaneous inclusion of self-energy and vertex corrections shows that the above results remain qualitatively unchanged down to very low temperatures $T \ll \Delta_0$. It is argued that this form of the spectral functions implies the quasisplitting of the Fermi surface in the paramagnetic phase in the presence of strong ferromagnetic fluctuations.

I. INTRODUCTION

Non-Fermi-liquid behavior of correlated low-dimensional electron systems has attracted much attention during the last decade. This behavior is usually connected with the violation of the quasiparticle (qp) concept in some energy window around the Fermi level. A prominent example is the pseudogap phenomenon observed in underdoped high-T_c compounds.[1] Cuprate superconductors are, however, not the only materials example which show a strong suppression of the low-energy spectral weight due to correlation effects. A qualitatively similar behavior on parts of the Fermi surfaces was also observed recently in the unconventional superconductor Sr_2RuO_4 in an intermediate-temperature range[2] and the layered manganite compound $La_{1+x}Sr_{2-x}Mn_2O_7$.[3]

One possible viewpoint for the origin of the pseudogap in high-T_c compounds is to relate it to precursors of antiferromagnetism.[4–6] The fluctuation exchange (FLEX),[7,8] two-particle self-consistent (TPSC),[9] dynamical cluster approximation,[10] and most recently the functional renormalization-group (fRG) technique[11,12] have demonstrated a strong anisotropy of spectral properties around the Fermi surface (FS) in the two-dimensional (2D) Hubbard model with a possible violation of the qp concept on parts of the FS. The large incoherent contributions to the electronic spectrum of low-dimensional metallic antiferromagnets (e.g., an anomalously large scattering rate) were also discussed in Ref. 13. These phenomena result in the formation of a two-[7–9,12] or three-peak[11] structure of the spectral function in the vicinity of the antiferromagnetic (AFM) instability. With decreasing temperature, these pseudogap features are expected to evolve continuously towards a ground state spectral function with an AFM energy gap at the Fermi level.

While many results have been obtained for the electronic properties in the vicinity of an AFM state and some results exist for itinerant ferromagnets,[14,15] surprisingly much less is known about the evolution of the quasiparticle properties in the paramagnetic phase near the ferromagnetic (FM) instability. The paramagnon theory[16–19] focused mostly on the description of the magnetic properties, ignoring the renormalization of the one-particle Green function. Nevertheless, already Doniach and Engelsberg[20] showed that in three dimensions the qp weight vanishes logarithmically on approaching a FM zero-temperature quantum phase transition (QPT). For two-dimensional (2D) systems, an $\varepsilon^{2/3}$ energy dependence of the self-energy at the quantum critical point (QCP) can be inferred from similar calculations in the context of gauge field theories,[21] the phase separation problem,[22] and the Pomeranchuk instability.[23] The latter two instabilities arise also in the zero-momentum transfer particle-hole channel and therefore are expected to have properties which are similar to those in the vicinity of the ferromagnetic QPT, at least in lowest order perturbation theory with respect to the fermion-boson (charge or spin modes) coupling. The $\varepsilon^{2/3}$ frequency dependence of the self-energy implies the vanishing of the qp weight at the Fermi level and therefore invalidates the qp concept. This may raise doubts about the validity of the applied scheme, since the abovementioned calculations did not consider both self-energy *and* vertex corrections. However, the calculations by Altshuler *et al.*[24] within the gauge field theory context showed that the $\varepsilon^{2/3}$ dependence of the self-energy remains valid also in higher orders of perturbation theory.

The breakdown of the qp concept at the QCP may be even more apparent at finite temperatures. For fermions interacting with a gauge field it was shown that for the case of gapless (although diffusive) bosonic excitations the imaginary part of the self-energy in a non-self-consistent calculation is divergent at the Fermi level at $T > 0$ as a consequence of the diverging static spin susceptibility $\chi(\mathbf{0}, 0)$.[21] This divergence should necessarily have certain consequences for the zero-momentum particle-hole instabilities of fermion
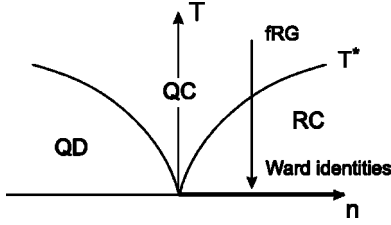
FIG. 1. Schematic picture for the three different temperature regimes near QPT, as proposed in Ref. 25: (1) the renormalized classical (RC) regime above the ordered ground state (indicated by the bold line, T^* is the corresponding crossover temperature scale discussed in the text), (2) the quantum disordered (QD) regime above a disordered ground state, and (3) the quantum critical (QC) regime. The arrow shows the direction, in which the evolution of the spectral properties is traced in this paper; "fRG" and "Ward identities" in the figure mark the intermediate ($T \gtrsim T^*$) and low-temperature ($T \ll T^*$) regimes, where the corresponding approaches are applied. The two-particle self-consistent approach is applied in both regimes.

systems with short-range interactions. Although the magnetic correlation length ξ of 2D systems with short-range interaction is finite at finite T and $\chi(\mathbf{0},0) \propto \xi^2$, three temperature regimes should be distinguished[25] (see Fig. 1): (i) the quantum disordered regime with a disordered ground state and almost temperature-independent correlation length, (ii) the quantum critical (QC) regime with $\xi \sim 1/T^\alpha$, and (iii) the renormalized-classical (RC) regime above an ordered ground state with an exponentially large correlation length at low T. The divergence of the imaginary part of the self-energy for $\xi \to \infty$ may lead to especially strong effects in the RC regime, where the inverse correlation length is almost negligibly small at low T. Indeed, for the AFM instability this divergence results in the formation of a pseudogap structure in the spectral function.[9] Although similar properties in the vicinity of a FM instability were discussed quite recently,[26,27] the behavior in this case is far less from clear, since the suppression of the spectral weight at the Fermi level itself weakens the tendency to ferromagnetic order, which therefore implies the necessity to account for self-energy and vertex corrections self-consistently.

The recently found nonanalytic contributions to the spin susceptibility in second-order perturbation theory with respect to the electron-electron interaction[28] have led to infer the possible absence of a second-order FM QPT, which is either replaced by a first-order transition to ferromagnetic phase or a second-order QPT into an incommensurate phase with a finite ordering wave vector $\mathbf{Q}$, which then continuously decreases towards $\mathbf{Q}=\mathbf{0}$ on moving away from the QPT into the ordered state. However, these corrections are not expected, at least in the weak-coupling regime, to remove the renormalized classical temperature regime entirely. Indeed, the corresponding characteristic temperature scale $T_X \sim (U/4\pi t)^2 t$, below which these corrections become important,[28] is quadratic in the interaction and therefore small in the weak-coupling regime in comparison with both the bandwidth and the crossover temperature $T^* \sim U$ into the renormalized classical temperature regime not too close to the QPT

It therefore appears demanding to investigate the finite-temperature behavior of the self-energy in the vicinity of the

FM instability and to compare non-self-consistent and self-consistent techniques. For non-self-consistent calculations, the TPSC as well as the recently proposed fRG approaches on a patched FS (Refs. 29–32) can be used. The latter approaches have the advantage that they do not select certain types of electronic scattering processes, but consider them all on equal footing. The self-consistent treatment of self-energy and vertex corrections is *per se* a rather difficult task. Most consistently this can be done in a parquet-type analysis[33] (see also Refs. 34 and 35), which is, however, necessarily rather involved for numerical studies in dimensions $d > 1$. In the fRG technique the back influence of the self-energy on one- and two-particle properties requires to work at two-loop order, which is currently inachievable. To obtain qualitative results deep inside the RC regime, the application of Ward identities offers an alternative. This strategy was chosen previously by Edwards and Hertz[14] to calculate the spin-resolved self-energy in the ordered FM phase. As we will show in this paper, an analogous approach can be similarly applied for magnetically disordered systems in the renormalized-classical regime.

In the present paper we use the TPSC, fRG, and Ward identity approaches to get insight from three different points of view into the behavior of the self-energy in 2D systems at finite temperatures on approaching the FM phase. First, in Sec. II we consider the main features of the self-energy obtained within the TPSC approximation and compare them with the results of the fRG approach, which is used to study in detail the frequency dependence of the self-energy at van Hove (vH) band fillings. In Sec. III we make use of Ward identities for a qualitative insight into the role of self-energy and vertex corrections at low temperatures.

II. THE SELF-ENERGY IN NON-SELF-CONSISTENT APPROACHES

Specifically we consider the Hubbard model for N_e electrons on a square lattice

$$H = -\sum_{ij\sigma} t_{ij} c_{i\sigma}^\dagger c_{j\sigma} + U \sum_i n_{i\uparrow} n_{i\downarrow} - (\mu - 4t') N_e, \quad (1)$$

where the hopping amplitude is $t_{ij} = t$ for nearest-neighbor sites i and j and $t_{ij} = -t'$ for next-nearest-neighbor sites $(t,t' > 0)$; for further convenience we have shifted the chemical potential μ by $4t'$; the corresponding electronic dispersion is

$$\varepsilon_\mathbf{k} = -2t(\cos k_x + \cos k_y) + 4t'(\cos k_x \cos k_y + 1) - \mu. \quad (2)$$

Furthermore we compare some of our results for the Hubbard model with those for the ferromagnetic s-d model[36,37]

$$H = -\sum_{ij\sigma} t_{ij} c_{i\sigma}^\dagger c_{j\sigma} - I \sum_i \mathbf{S}_i \cdot \boldsymbol{\sigma}_{\sigma\sigma'} c_{i\sigma}^\dagger c_{i\sigma'}$$

$$- \frac{1}{2} \sum_{ij} J_{ij} \mathbf{S}_i \cdot \mathbf{S}_j - (\mu - 4t') N_e \quad (3)$$

in the weak-coupling regime $0 < I \ll 8t$, where $\mathbf{S}_i$ are

localized-spin operators and $\boldsymbol{\sigma}_{\sigma\sigma'}$ are Pauli matrices; $J_{ij}=J>0$ is the direct nearest-neighbor ferromagnetic spin exchange coupling.

A. TPSC approximation

The TPSC approximation[9] for the Hubbard model (1) considers the dynamical spin susceptibility

$$\chi(\mathbf{q},\omega) = \frac{\chi_0(\mathbf{q},\omega)}{1 - U_{sp}\chi_0(\mathbf{q},\omega)} \tag{4}$$

which has the same structure as the spin susceptibility in the random-phase approximation (RPA), but contains an effective interaction U_{sp} instead of the bare U. The bare susceptibility $\chi_0(\mathbf{q},i\omega_n)$ is given by

$$\chi_0(\mathbf{q},i\omega_n) = \frac{1}{N}\sum_{\mathbf{k}} \frac{f_{\mathbf{k}} - f_{\mathbf{k}+\mathbf{q}}}{i\omega_n - \varepsilon_{\mathbf{k}} + \varepsilon_{\mathbf{k}+\mathbf{q}}}, \tag{5}$$

where $f_{\mathbf{k}}=f(\varepsilon_{\mathbf{k}})$ is the Fermi function and $\omega_n=2\pi nT$. The effective interaction U_{sp} is determined by the sum rule[9]

$$\frac{T}{N}\sum_{\mathbf{q},i\omega_n} \chi(\mathbf{q},i\omega_n) = n/2 - n^2 U_{sp}/(4U) \tag{6}$$

with $n=N_e/N$ being the band filling and k_B is set to unity. The renormalization of the interaction $U_{sp}/U<1$ avoids the artificial divergence of the susceptibility at finite temperature where the denominator of Eq. (4) calculated with the bare interaction U vanishes. The temperature and t' dependence of U_{sp} was extensively discussed in Refs. 9 and 26; U_{sp} decreases with increasing t' and decreasing temperature.

Above the ordered ground state the inverse correlation length in TPSC

$$\xi^{-1} \propto [1 - U_{sp}\chi_0(\mathbf{Q},0)]^{1/2} \tag{7}$$

monotonically decreases with temperature and becomes exponentially small, $\xi^{-1}=C\exp(-T^*/T)$, below a certain crossover temperature $T^*=4\pi A U_{sp}\overline{S}_0^2/(3\overline{\chi_0})$, where $\overline{\chi_0}=\chi_0(\mathbf{Q},0)$, $A=\nabla^2\chi_0(\mathbf{q},0)|_{\mathbf{q}=\mathbf{Q}}$, C is a constant, and

$$\overline{S}_0^2 = 3n/4 - 3n^2/(8U\overline{\chi_0}) - \frac{3}{2}\left[\frac{T}{N}\sum_{\mathbf{q},i\omega_n} \frac{\chi_0(\mathbf{q},i\omega_n)}{1 - \chi_0(\mathbf{q},i\omega_n)/\overline{\chi_0}}\right]_{T=0} \tag{8}$$

is the square of the ground-state (sublattice) magnetization per site, $\mathbf{Q}$ is the magnetic ordering wave vector, determined by the maximum of $\chi_0(\mathbf{Q},0)$. In the following we suppose $\mathbf{Q}=0$, which corresponds to a ferromagnetic instability and is in particular the case for van Hove (vH) band fillings ($\mu=0$) of the t-t' Hubbard model, Eq. (1), with $0.3t \lesssim t' < 0.5t$.[26,32,38] Note that here we ignore the possibility of triplet pairing, which may also arise in the vicinity of the FM instability.[32]

The self-energy is given by

$$\Sigma(\mathbf{k},i\varepsilon_n) = \frac{UU_{sp}T}{2N}\sum_{\mathbf{q},i\omega_n} [3\chi(\mathbf{q},i\omega_n) - \chi_0(\mathbf{q},i\omega_n)]$$

$$\times \frac{1}{i\varepsilon_n + i\omega_n - \varepsilon_{\mathbf{k}+\mathbf{q}}} \tag{9}$$

on the imaginary frequency axis [$\varepsilon_n=(2n+1)\pi T$ are fermionic Matsubara frequencies] and

$$\Sigma(\mathbf{k},\varepsilon + i0^+) = \frac{UU_{sp}}{2N}\sum_{\mathbf{q}} \int d\omega[3\,\mathrm{Im}\,\chi(\mathbf{q},\omega) - \mathrm{Im}\,\chi_0(\mathbf{q},\omega)]$$

$$\times \frac{N_B(\omega) + f(\varepsilon_{\mathbf{k}+\mathbf{q}})}{\varepsilon + \omega - \varepsilon_{\mathbf{k}+\mathbf{q}} + i0^+} \tag{10}$$

on the real axis, where $N_B(\omega)$ is the Bose distribution function. The factor 3 in the first term in the square brackets of Eqs. (9) and (10) arises from the summation over three (two transverse and one longitudinal) spin channels, the second term in the square brackets is substracted to avoid double counting of the second-order diagram.

The same expressions (9) and (10) with the replacement $UU_{sp}\to I^2$ hold for the s-d model (3) in second order perturbation theory with respect to the electron-spin interaction I, see, e.g., Ref. 15. The magnetic correlations in this case originate mainly from the exchange interaction between the localized spins, and the magnetic susceptibility has the same form as for the Heisenberg model with nearest neighbor exchange interaction J. The inverse magnetic correlation length at low T is again exponentially small,[39] $\xi^{-1}=C\exp(-JS^2/T)$; the corresponding crossover temperature into the RC regime is $T^* \sim JS^2$.

To calculate the self-energy at small ε and $\mathbf{k}$ near the Fermi surface, we expand the bare susceptibility χ_0 at small q and ω For the Hubbard model at $\mu \neq 0$ the resulting spin susceptibility on the real frequency axis is given by (see, e.g., Ref. 18)

$$\chi(\mathbf{q},\omega) = \frac{\chi_0}{A(q^2 + \xi^{-2}) + iB\omega/q}, \tag{11}$$

where the correlation length ξ in TPSC is given by Eq. (7), A and B are constants which are proportional to U_{sp} with a coefficient which depends on the bare spectrum $\varepsilon_{\mathbf{k}}$ (see Ref. 18 for explicit expressions). For the van Hove singularity (vHs) case ($\mu=0$) we obtain

$$\chi(\mathbf{q},\omega) = \frac{\chi_0}{A(q^2 + \xi^{-2}) + i\Gamma(q_\pm,\omega)}, \tag{12}$$

where (cf. the $T=t'=0$ result of Ref. 40)

$$\Gamma(q_\pm,\omega) = \frac{U_{sp}}{2\pi t \sin^2 2\varphi} \frac{\omega}{\max[\omega,(Tt|q_+q_-|)^{1/2},t|q_+q_-|]} \tag{13}$$

is the damping of the spin excitations, $q_\pm = q_x \sin\varphi \pm q_y \cos\varphi$, and $\cos 2\varphi = 2t'/t$.

The form of the dynamic magnetic susceptibility of the s-d model in the paramagnetic phase, which is mostly determined by the local moment subsystem, is more complicated.

TABLE I. Inverse quasiparticle lifetime $\tau^{-1}(\mathbf{k}_F)$ and $[\partial \operatorname{Re} \Sigma(\mathbf{k}_F, \varepsilon)/\partial \varepsilon]_{\varepsilon=0}$ in second-order perturbation theory (SOPT) and the two-particle self-consistent approximation (TPSC) near the FM instability for different bare electronic spectra.

Spectrum	$\tau^{-1}(\mathbf{k}_F)$		$[\partial \operatorname{Re} \Sigma(\mathbf{k}_F, \varepsilon)/\partial \varepsilon]_{\varepsilon=0}$	
	SOPT	TPSC	SOPT	TPSC
Linear $(\mu \neq 0)$	$(T^2/t)\ln(1/T)$	$T\xi + tO[(T/t)^{2/3}]$	const < 0	$(T/t)\xi^2 + O[(T/t)^{1/3}]$
vHs $(\mu = 0)$ $\begin{cases} \mathbf{k} = \mathbf{k}_{\mathrm{vH}} \\ \mathbf{k} \neq \mathbf{k}_{\mathrm{vH}} \end{cases}$	$T\ln(1/T)$ $(T^2/t)\ln(1/T)$	$T\xi^2 + tO[(T/t)^{2/3}]$ $T\xi + tO[(T/t)^{5/6}]$	$\ln(1/T)$ const < 0	$(T/t)\xi^4 + O[(T/t)^{1/3}]$ $(T/t)\xi^2 + O[(T/t)^{2/3}]$

However, we will see below that already the static part of the susceptibility dominates the spectral properties at low $T \lesssim T^*$. In the static limit the susceptibility in the RC regime is expected to coincide with that determined for the AFM case within a $1/M$ expansion in the $O(M)$ Heisenberg model[41] and has the same form as Eq. (11) with $\omega = 0$.

To analyze spectral properties, we first consider the inverse qp lifetime

$$\frac{1}{\tau(\mathbf{k}_F)} = -\operatorname{Im} \Sigma(\mathbf{k}_F, i0^+)$$

$$= -\frac{\pi U U_{\mathrm{sp}}}{2N} \sum_{\mathbf{q}} \frac{3\operatorname{Im}\chi(\mathbf{q}, \varepsilon_{\mathbf{k}_F+\mathbf{q}}) - \operatorname{Im}\chi_0(\mathbf{q}, \varepsilon_{\mathbf{k}_F+\mathbf{q}})}{\sinh(\varepsilon_{\mathbf{k}_F+\mathbf{q}}/T)}$$

(14)

and the derivative of the real part of the self-energy at the Fermi level

$$\left.\frac{\partial \operatorname{Re}\Sigma(\mathbf{k}_F, \varepsilon)}{\partial \varepsilon}\right|_{\varepsilon=0} = -\frac{U U_{\mathrm{sp}}}{2N}\mathcal{P}\int d\omega \sum_{\mathbf{q}} [3\operatorname{Im}\chi(\mathbf{q}, \omega)$$

$$- \operatorname{Im}\chi_0(\mathbf{q}, \omega)]\frac{N_B(\omega) + f(\varepsilon_{\mathbf{k}_F+\mathbf{q}})}{(\omega - \varepsilon_{\mathbf{k}_F+\mathbf{q}})^2}.$$

(15)

The results for the leading terms at $T \ll t$ together with the results of second-order perturbation theory (SOPT) [which is obtained by the replacement $\chi \rightarrow \chi_0$ in Eq. (14)] are collected in Table I, where we omit overall temperature-independent prefactors which are proportional to U^2/t^2.

Apparently, the imaginary part of the self-energy at the Fermi level is anomalously enhanced by the correlation effects for $\xi \gg 1$ and even tends to diverge deep inside the RC regime $T \ll T^*$, where $\xi \rightarrow \infty$. Simultaneously, $\partial \operatorname{Re}\Sigma/\partial\varepsilon|_{\varepsilon=0}$ becomes positive and large. At energies $|\omega| \gtrsim t\xi^{-1}$ ($t\xi^{-2}$ in the vHs case) the real part of the self-energy behaves as Δ_0^2/ω, where $\Delta_0 = (U U_{\mathrm{sp}})^{1/2}\bar{S}_0 \sim T^*$. It is worthwhile to note that the abovementioned divergencies arise from the purely static contributions with zero bosonic Matsubara frequency and were previously discussed in detail for the AFM case in Refs. 6 and 9, where $\bar{S}_0$ is the ground-state sublattice magnetization.

These low-energy features lead to a suppression of spectral weight in $A(\mathbf{k}, \omega) = -(1/\pi)\operatorname{Im}\Sigma/[(\omega - \varepsilon_{\mathbf{k}} + \operatorname{Re}\Sigma)^2 + (\operatorname{Im}\Sigma)^2]$ at $|\omega| \lesssim \Delta_0$ (see also Ref. 26) and to the formation of a two-peak structure of the spectral function with the

peaks located near $\omega \simeq \pm \Delta_0$. While for the AFM case the fulfillment of the nesting condition $\varepsilon_{\mathbf{k}_F+\mathbf{Q}} = -\varepsilon_{\mathbf{k}_F} = 0$ (which for $t' \neq 0$ is satisfied only at the hot spots) is required, in the FM case the two-peak structure occurs all around the FS. The difference between the FM and AFM instabilities at those points where $\varepsilon_{\mathbf{k}_F+\mathbf{Q}} = 0$ is evident only in the subleading terms $\sim T^\alpha$, where the exponent α depends on the dynamical exponent z [e.g., $\tau^{-1}(\mathbf{k}_F) \sim T\xi + tO(T/t)^{1-1/z}$ and $[\partial \operatorname{Re}\Sigma/\partial\varepsilon|_{\varepsilon=0} \sim (T/t)\xi^2 + O(T/t)^{1-2/z}$ for the linear electronic dispersion near the Fermi level], $z=2$ for the AFM and $z=3$ for the FM case. Note that unlike Refs. 9 and 26 we did not suppose that $T \ll T^*$ in deriving the results of Table I, and in fact these results are valid for both RC and QC regimes.

The above discussed features of the self-energy keep their form away from the FS with the replacement $\varepsilon \rightarrow \varepsilon - \varepsilon_{\mathbf{k}+\mathbf{Q}}$. This holds for all $|\varepsilon_{\mathbf{k}+\mathbf{Q}}| \ll t$ for a linear electronic dispersion and for $t\xi^{-2} \ll |\varepsilon_{\mathbf{k}+\mathbf{Q}}| \ll t$ for vH band fillings. At vH band fillings and $|\varepsilon_{\mathbf{k}+\mathbf{Q}}| \lesssim t\xi^{-2}$ additional divergent terms in the real part of the self-energy arise at the vH points $\mathbf{k}_{\mathrm{vH}} = (0, \pi)$ and $(\pi, 0)$ with $\operatorname{Re}\Sigma(\mathbf{k}_{\mathrm{vH}}, 0) \sim tk_+k_-\xi^4$ [$k_{\pm} = (k_x - \pi)\sin\varphi \pm k_y \cos\varphi$ for $\mathbf{k}_{\mathrm{vH}} = (\pi, 0)$ and similarly for the other vH point], which flatten the bare electronic dispersion at the momenta near $\mathbf{k}_{\mathrm{vH}}$, similar to the zero temperature case.[42] This flattening, however, is not important in the RC regime since the corresponding momentum region is rather narrow and $\operatorname{Im}\Sigma$ at the Fermi level is finite at finite T (and even diverges at $\xi \rightarrow \infty$).

The dependence on $\varepsilon - \varepsilon_{\mathbf{k}+\mathbf{Q}}$ for $t\xi^{-2} \ll |\varepsilon_{\mathbf{k}+\mathbf{Q}}| \ll t$ is the origin for an important difference between the spectral functions near the FM and AFM instabilities *away* from the FS. In the FM case the spectral functions depend on $\varepsilon - \varepsilon_{\mathbf{k}}$ only, implying that at $\varepsilon_{\mathbf{k}} \simeq \pm \Delta_0$ (the condition which determines the FSs of spin-up and spin down electrons in the FM phase) one of the peaks of the above discussed two-peak structure is located at the Fermi level, making the electronic excitations at the points of the Brillouin zone with $\varepsilon_{\mathbf{k}} \simeq \pm \Delta_0$ coherent. This indicates the existence of two "preformed" Fermi surfaces already in the paramagnetic (PM) phase at low temperatures $T \lesssim T^*$. The corresponding electronic excitations, however, do not have any prefered spin direction and the spin symmetry remains necessarily unbroken at $T > 0$. As we show in Sec. III, self-consistent approaches show the same tendency of the spectral weight suppression at the PM Fermi surface, and the redistribution of spectral weight towards the energies $\omega \simeq \pm \Delta_0$ supports therefore the picture described above in the non-self-consistent TPSC analysis.

B. fRG analysis at van Hove band fillings

The two-particle self-consistent approximation may be insufficient close to van Hove band fillings since it considers only the contribution of particle-hole excitations and the other electronic scattering channels are accounted for only by the "average" renormalized interaction U_{sp}. Moreover, at van Hove band fillings the effective interaction U_{sp} artificially tends to zero with decreasing temperature (see, e.g., Ref. 9). To analyze in more detail the frequency dependence of the self-energy in the vicinity of van Hove band fillings, we apply the fRG approach for one particle-irreducible (1PI) functions[31] with a temperature cutoff.[32] This approach considers the evolution of the generating functional with decreasing temperature in the weak-coupling regime. The flow of the self-energy $\Sigma_T(\mathbf{k}, i\omega) = T^{-1/2} \Sigma(\mathbf{k}, i\omega)$ in the 1PI fRG scheme is given by

$$\frac{d\Sigma_T}{dT} = V_T \circ S_T, \qquad (16)$$

where $\circ$ is a short notation for the summation over momentum, frequency, and spin variables according to standard diagrammatic rules, see, e.g., Ref. 43. The renormalization of the electron-electron interaction vertex V_T at one-loop order is given by

$$\frac{dV_T}{dT} = V_T \circ (G_T \circ S_T + S_T \circ G_T) \circ V_T. \qquad (17)$$

The propagators G_T and S_T are defined by

$$G_T(\mathbf{k}, i\nu_n) = \frac{T^{1/2}}{i\nu_n - \varepsilon_{\mathbf{k}}}, \quad S_T(\mathbf{k}, i\nu_n) = -\frac{1}{2T^{1/2}} \frac{i\nu_n + \varepsilon_{\mathbf{k}}}{(i\nu_n - \varepsilon_{\mathbf{k}})^2}. \qquad (18)$$

The factors $T^{1/2}$ arise due to the rescaling of the fermion fields on removing the temperature dependence from the interaction term of the action.[32] Equations (16) and (17) have to be solved with the initial conditions $V_{T_0} = U$ and $\Sigma_{T_0} = 0$ where $T_0 \gg t$. In the non-self-consistent treatment in this section we have neglected the self-energy in the denominators of the Green functions (18). The self-consistent RG analysis is rather involved and requires the inclusion of two-loop corrections which remain a challenging task for fRG techniques.

Since the frequency dependence of the vertices is neglected in the calculations, it is convenient to reinsert, following Ref. 43, the vertex from Eq. (17) into Eq. (16) to obtain

$$\frac{d\Sigma_T}{dT} = S_T \circ \int_T^{T_0} dT' [V_{T'} \circ (G_{T'} \circ S_{T'} + S_{T'} \circ G_{T'}) \circ V_{T'}]. \qquad (19)$$

To avoid the integration over temperature in the right-hand side of Eq. (19) we integrate by parts to obtain (cf. Ref. 43 for the momentum-cutoff scheme)

$$\frac{d\Sigma_T}{dT} = (G_T - G_{T_f}) \circ [V_T \circ (G_T \circ S_T + S_T \circ G_T) \circ V_T], \qquad (20)$$

where T_f is the final temperature where the self-energy is evaluated. Although Eq. (20) contains the Matsubara sums of the Green functions at different temperatures, these sums can be calculated by the same procedure as for equal-temperature Green functions.

To solve Eqs. (17) and (20) numerically we divide the momentum space into 32 patches with the same patching scheme as in Refs. 31 and 32. To calculate the self-energy on the real frequency axis we use analytical continuation by Padé approximants.[44] Similar to Ref. 11 we use the advantage of Eq. (19) that for frequency-independent vertices, after analytical summation over internal frequencies, the self-energy can be calculated at arbitrary frequencies on the imaginary axis, and therefore we choose a mesh on the frequency axis, which becomes denser close to $i\omega = 0$.[11]

We consider the results at the vH band filling ($\mu = 0$) for $t' = 0.45t$ and $U = 4t$ where ferromagnetism is expected in the ground state.[32,38] We choose this relatively large value of U because the crossover temperatures T^* for the FM instability are smaller then for the AFM case ($T^* \lesssim 0.1t$ for the parameters we use), and for lower values of U and correspondingly lower temperatures the analytical continuation becomes increasingly difficult, since the size of the anomalous frequency region in the vicinity of the Fermi level decreases with T^*. The SOPT self-energy[which is obtained by the replacement $V \to U$ in Eq. (19)] calculated at temperatures $T = 0.1t$, $0.3t$ and $0.5t$ for $\mathbf{k}_F = (2.83, 0.07)$, which is the center of the first patch, closest to the $(\pi, 0)$ point, is shown in Fig. 2. The SOPT self-energy at other points on the FS looks similar. As in the AFM case[11] at high temperatures $T \gtrsim 0.3t$ the self-energy has a sharp dip at the Fermi level due to vH singularity effects. Im $\Sigma^{(\text{SOPT})}(\mathbf{k}_F, 0)$ decreases with decreasing temperature and Im $\Sigma(\mathbf{k}_F, 0) = 0$ at $T = 0$. This, however, does not imply the validity of the qp picture everywhere on the Fermi surface since Im $\Sigma(\mathbf{k}_F, \varepsilon) \propto \varepsilon \ln(1/\varepsilon)$ for the vH points $\mathbf{k}_F = (\pi, 0)$ and $(0, \pi)$ at $T = 0$,[40] although the "normal" 2D behavior Im $\Sigma(\mathbf{k}_F, \varepsilon) \propto \varepsilon^2 \ln(1/\varepsilon)$ (Ref. 45) is restored for other points of the Fermi surface.

The self-energy obtained within the fRG technique for the temperatures $T = 0.1t$ and $T = 0.3t$ is shown in Figs. 3–5. The results for $T = 0.5t$ (not shown) are similar to those at $T = 0.3t$ and both are close to the results of the SOPT, Fig. 2. But in contrast to SOPT, with decreasing temperature to $T = 0.1t$ a new sharp feature appears in a narrow region near the Fermi level (Fig. 4). Note that the maximum effective interaction $V_{\max} \equiv \max\{V(\mathbf{k}_1, \mathbf{k}_2; \mathbf{k}_3, \mathbf{k}_4)\} = 20t$ for this temperature. Similarly to the TPSC approach of Sec. II A, the imaginary part of the self-energy has a minimum at the Fermi level instead of a maximum as expected for a Fermi liquid. Simultaneously, Re $\Sigma(\mathbf{k}_F, \omega)$ has a positive slope near $\omega = 0$. These pronounced anomalies in the fRG self-energy increase in size with decreasing T and lead to a suppression of spectral weight at the Fermi energy. The spectral function [Fig. 4(d)] has an asymmetric two-peak structure. A qualitatively similar picture is observed in the fourth FS patch, clos-
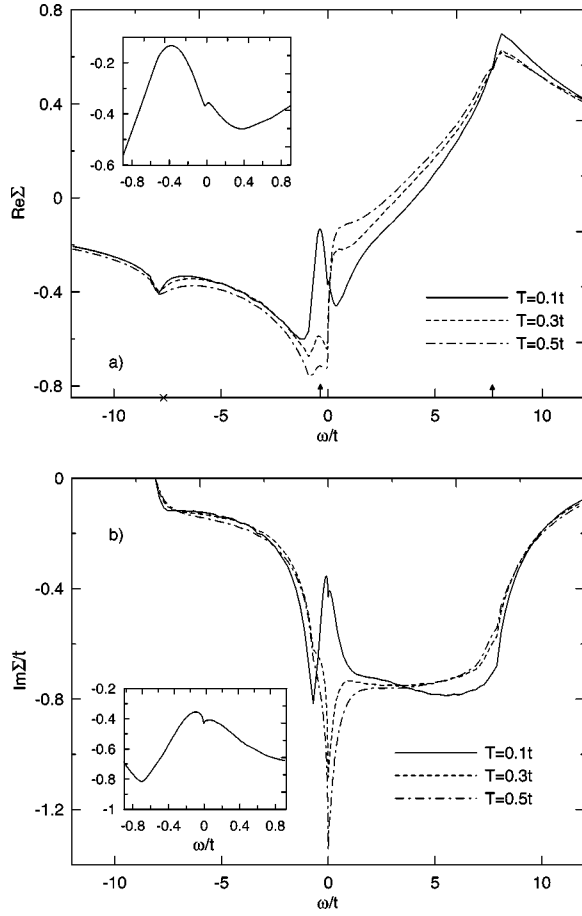
FIG. 2. The real (a) and imaginary (b) parts of the self-energy in second-order perturbation theory (SOPT) at $t'/t=0.45$, $U=4t$, $\mu=0$ (vH band filling), and different temperatures. Arrows mark the energy of the lower and upper edges of the noninteracting band ($\varepsilon_{\min}=-4+8t'$ and $\varepsilon_{\max}=4+8t'$, respectively), the cross marks the energy, opposite to the upper edge of the band $-\varepsilon_{\max}$. The insets show the behavior of ReΣ and ImΣ at low energies for $T=0.1t$.

est to the Brillouin zone diagonal with $\mathbf{k}_F=(1.06,0.75)$ (Fig. 5) where at low temperatures the fRG result also leads to a two-peak structure of the spectral function, where, however, the $\omega>0$ peak is larger than $\omega<0$ one.

The magnitude of Re $\Sigma(\mathbf{k}_F,0)\simeq-0.4t$ in the first, closest to $(\pi,0)$ patch of the FS is almost the same in both the SOPT and fRG approaches, and is much larger than the corresponding value found in the vicinity of the AFM instability.[11] At the same time, in the fourth patch of the FS, the fRG approach gives slightly positive Re $\Sigma(\mathbf{k}_F,0)$, while Re $\Sigma(\mathbf{k}_F,0)$ in SOPT approach remains almost patch independent. Therefore, the fRG approach, in contrast to SOPT, leads to a significant deformation of the FS near the FM instability at vH band fillings, which reflects a band narrowing tendency; in essence, the effective (renormalized) value of the next-nearest-neighbor hopping t' increases towards its value in the flat-band case $t'/t=1/2$ (see, e.g., the discussion in Ref. 38). This is similar to the earlier discussed flattening of the dispersion close to $(\pi,0)$ and $(0,\pi)$ points at vH band fillings,[42] except that in the present case the flattening affects larger parts of the Brillouin zone along the zone axes. The
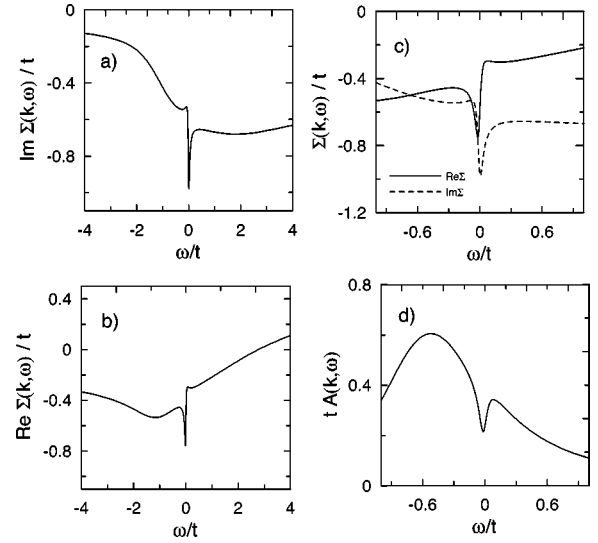

FIG. 3. The functional renormalization group results for the self-energy (a)–(c) and the spectral function (d) in the first Fermi surface patch, closest to the $(\pi,0)$ point at $t'/t=0.45$, $U=4t$, $\mu=0$, and $T=0.3t$.

sizable value of $|\mathrm{Re}\,\Sigma|$ at the Fermi surface leads to an asymmetric shape of the spectral functions in the vicinity of the Fermi energy, in contrast to the analytical approach of Sec. II A, where this FS shift was not taken into account.

III. THE SELF-CONSISTENT APPROACH AT $T\ll T^*$

To get qualitative insight into the role of self-consistency effects below T^*, we consider the general form of the spin susceptibilities

$$\chi^{+-}(\mathbf{q},i\omega_n)=-\frac{2T}{N}\sum_{\mathbf{k},i\nu_n}\Gamma^+_{\uparrow\downarrow}(\mathbf{k},\mathbf{k}+\mathbf{q};i\nu_n,i\nu_n+i\omega_n)G_\uparrow(\mathbf{k},i\nu_n)$$

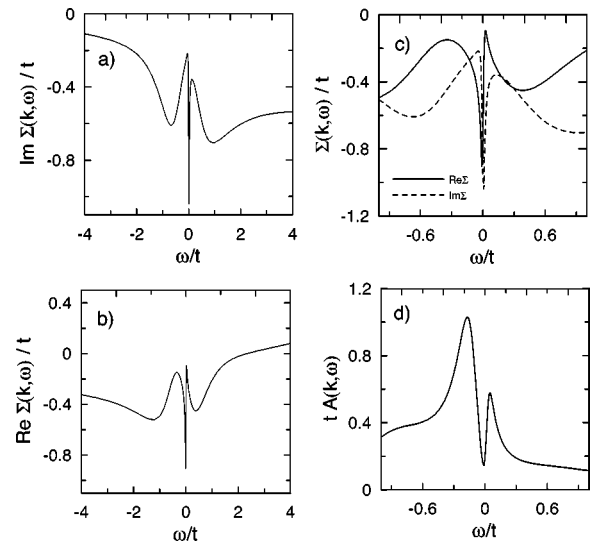$$\times G_\downarrow(\mathbf{k}+\mathbf{q},i\omega_n+i\nu_n),$$
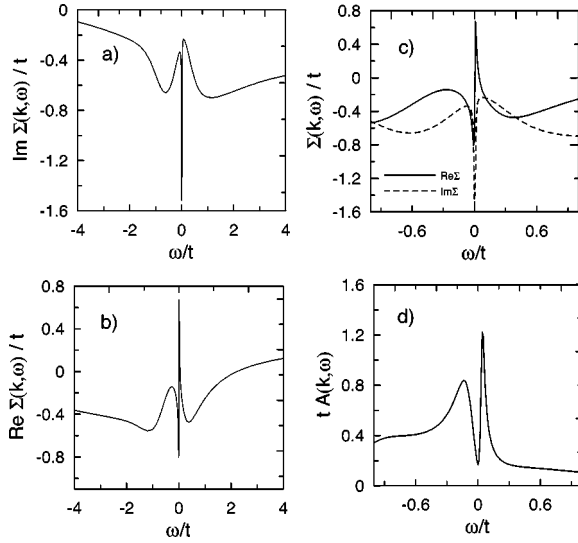

FIG. 4. Same as Fig. 3 for $T=0.1t$.

FIG. 5. Same as Fig. 3 for $T=0.1t$ in the fourth Fermi surface patch closest to the Brillouin zone diagonal.

$$\chi^{zz}(\mathbf{q},i\omega_n) = -\frac{T}{N}\sum_{\mathbf{k},i\nu_n}\Gamma^z_{\uparrow\uparrow}(\mathbf{k},\mathbf{k}+\mathbf{q};i\nu_n,i\nu_n+i\omega_n)$$

$$\times G_\uparrow(\mathbf{k},i\nu_n)G_\uparrow(\mathbf{k}+\mathbf{q},i\omega_n+i\nu_n), \qquad (21)$$

where

$$\Gamma^a_{\sigma\sigma'}(\mathbf{k},\mathbf{k}',i\nu_n,i\nu'_n) = G^{-1}_\sigma(\mathbf{k},i\nu_n)G^{-1}_{\sigma'}(\mathbf{k}',i\nu'_n)$$

$$\times \int_0^{1/T}\int_0^{1/T} e^{i(\nu_n\tau+\nu'_n\tau')}$$

$$\times \langle T[S^a_{\mathbf{k}-\mathbf{k}'}(0)c^\dagger_{\mathbf{k}\sigma}(\tau)c_{\mathbf{k}',\sigma'}(\tau')]\rangle d\tau d\tau'$$

$$\tag{22}$$

are the three-point spin vertex functions and $S^a_{\mathbf{q}}(\tau) = (1/N)\sum_{\mathbf{k}}c^\dagger_{\mathbf{k}\alpha}(\tau)\sigma^a_{\alpha\beta}c_{\mathbf{k}+\mathbf{q},\beta}(\tau)$. We retain the spin indices in this section to perform calculations in the presence of a small static external Zeeman field h which is set to zero at the end. To arrive at the RPA-like form of the susceptibilities, we follow Ref. 14 and introduce the irreducible vertices $\gamma^a_{\sigma\sigma'}$

$$\gamma^a_{\sigma\sigma'}(\mathbf{k},\mathbf{k}',i\nu_n,i\nu'_n) = \frac{\Gamma^a_{\sigma\sigma'}(\mathbf{k},\mathbf{k}',i\nu_n,i\nu'_n)}{1+U\chi^{a\bar{a}}(\mathbf{k}-\mathbf{k}',i\nu_n-i\nu'_n)} \qquad (23)$$

($\bar{a}=z$ for $a=z$ and $\bar{a}=-$ for $a=+$) to obtain

$$\chi^{ab}(\mathbf{q},i\omega_n) = \frac{\phi^{ab}(\mathbf{q},i\omega_n)}{1-U\phi^{ab}(\mathbf{q},i\omega_n)}, \qquad (24)$$

where $a,b=+,-,z$, and the function ϕ^{ab} has the same structure as χ^{ab} in Eq. (21) with the replacement $\Gamma\rightarrow\gamma$. Note that

$$\gamma^+_{\uparrow\downarrow} = \gamma^-_{\downarrow\uparrow} = \tilde{\gamma}^z_{\uparrow\uparrow} = \tilde{\gamma}^z_{\downarrow\downarrow}; \chi^{+-} = 2\chi^{zz}$$

(and similar for Γ) at $h=0$.

The expression for the self-energy, including the Hartree term, reads

$$\Sigma_\sigma(\mathbf{k},i\nu_n) = -\frac{TU}{N}\sum_{\mathbf{k}',i\nu'_n}G_\sigma(\mathbf{k}',i\nu'_n) + \frac{TU^2}{N}\sum_{\mathbf{q},i\omega_n}[\gamma^z_{\sigma,\sigma}(\mathbf{k},\mathbf{k}$$

$$+\mathbf{q};i\nu_n,i\nu_n+i\omega_n)G_\sigma(\mathbf{k}+\mathbf{q},i\omega_n+i\nu_n)\chi^{zz}(\mathbf{q},i\omega_n)$$

$$+\gamma^+_{\sigma,-\sigma}(\mathbf{k},\mathbf{k}+\mathbf{q};i\nu_n,i\nu_n+i\omega_n)G_{-\sigma}(\mathbf{k}+\mathbf{q},i\omega_n$$

$$+i\nu_n)\chi^{+-}(\mathbf{q},i\omega_n)]. \qquad (25)$$

We neglected the contribution of charge excitations here, which are not singular near the magnetic phase transition.

We note that a similar expression for the self-energy can be obtained for the ferromagnetic s-d model (3) but in this case the susceptibilities $\chi^{zz}(\mathbf{q},i\omega_n)$ and $\chi^{+-}(\mathbf{q},i\omega_n)$ are determined by the localized-moment subsystem. This difference, however, will not be important in the following sequence of arguments and the results of this section are applicable for this model as well.

As discussed in Sec. II A, the main contribution to Eq. (22) comes from the bosonic Matsubara frequency $i\omega_n=0$. The vertex $\Gamma^a_{\sigma,\sigma'}(\mathbf{k},\mathbf{k}+\mathbf{q};i\nu_n,i\nu_n)$ in the limit $\mathbf{q}\rightarrow\mathbf{0}$ [which we denote in the following as $\Gamma^a_{\sigma,\sigma'}(\mathbf{k},\mathbf{k};i\nu_n,i\nu_n)$ and similarly for γ] is found from a Ward identity. The standard Ward identity (see, e.g., Ref. 46)

$$\lim_{\omega\rightarrow 0}\Gamma^a_{\sigma\sigma'}(\mathbf{k},\mathbf{k};i\nu_n,i\nu_n+i\omega)$$

$$= \sigma^a_{\sigma\sigma'}[1-\partial\Sigma(\mathbf{k},i\nu_n+i\omega)/\partial(i\omega)]_{\omega=0} \qquad (26)$$

is not appropriate for that purpose since it considers the opposite order of limits for the vertex $\lim_{\omega\rightarrow 0}\lim_{q\rightarrow 0}\Gamma$ as required for the calculations in the RC regime. Instead, we use the identity of Ref. 14 to obtain for $h\rightarrow 0$

$$\Gamma^+(\mathbf{k},\mathbf{k};i\nu_n,i\nu_n) = \Gamma^z(\mathbf{k},\mathbf{k};i\nu_n,i\nu_n) = 1+\left.\frac{\Sigma_\uparrow(\mathbf{k},i\nu_n)-\Sigma_\downarrow(\mathbf{k},i\nu_n)}{h}\right|_{h=0} \simeq 1-\frac{TU}{N}\sum_{\mathbf{q},i\omega_n}G^2(\mathbf{k}',i\nu'_n)\Gamma(\mathbf{k}',\mathbf{k}';i\nu'_n,i\nu'_n)$$

$$+\frac{TU^2}{N}\sum_{\mathbf{q},i\omega_n}\left\{\gamma(\mathbf{k},\mathbf{k}+\mathbf{q};i\nu_n,i\nu_n+i\omega_n)\Gamma(\mathbf{k}+\mathbf{q},\mathbf{k}+\mathbf{q};i\nu_n+i\omega_n,i\nu_n+i\omega_n)G^2(\mathbf{k}+\mathbf{q},i\omega_n+i\nu_n)[\chi^{zz}(\mathbf{q},i\omega_n)\right.$$

$$\left.-\chi^{+-}(\mathbf{q},i\omega_n)]+\left[\frac{d}{dh}\gamma^z(\mathbf{k},\mathbf{k}+\mathbf{q};i\nu_n,i\nu_n+i\omega_n)\right]_{h=0}G(\mathbf{k}+\mathbf{q},i\omega_n+i\nu_n)\chi^{zz}(\mathbf{q},i\omega_n)\right\}, \qquad (27)$$

where we have denoted $\Gamma = \Gamma^+$, $\gamma = \gamma^+$, and we have omitted spin indices. Note that in the third and fourth line of Eq. (27) we have neglected h-derivatives of γ^+, χ^{+-}, and χ^{zz}. These derivatives lead to nonsingular contributions, at least for the linear dispersion case, which we mostly consider in the following. Using the relation (23) between Γ and γ and the relation (21) between Γ and χ we obtain from Eq. (27) the following integral equation for the vertex function γ:

$$\gamma(\mathbf{k},\mathbf{k};i\nu_n,i\nu_n) \simeq 1 + \frac{TU^2}{N} \sum_{\mathbf{q},i\omega_n} \left\{ \gamma(\mathbf{k},\mathbf{k}+\mathbf{q};i\nu_n,i\nu_n+i\omega_n) \right.$$
$$\times \gamma(\mathbf{k}+\mathbf{q},\mathbf{k}+\mathbf{q};i\nu_n+i\omega_n,i\nu_n+i\omega_n)$$
$$\times G^2(\mathbf{k}+\mathbf{q},i\omega_n+i\nu_n)[\chi^{zz}(\mathbf{q},i\omega_n)$$
$$- \chi^{+-}(\mathbf{q},i\omega_n)] + \frac{\chi^{zz}(\mathbf{q},i\omega_n)}{1+U\chi(\mathbf{q},i\omega_n)} \left[\frac{d}{dh}\gamma^z(\mathbf{k},\mathbf{k} \right.$$
$$+ \mathbf{q};i\nu_n,i\nu_n+i\omega_n) \bigg]_{h=0} G(\mathbf{k}+\mathbf{q},i\omega_n+i\nu_n) \bigg\}.$$

$$(28)$$

In principle, Eq. (28) is the first equation in an infinite hierarchy, since the calculation of $d\gamma^z/dh$ involves $d^2\gamma^z/dh^2$, etc. To close the system of equations in an approximate way, we proceed similarly to the $1/M$ expansion within the $O(M)$ generalization of the Heisenberg model for localized-moment systems.[41,47] Namely, we suppose that there are $M-1$ transverse spin modes and one longitudinal mode. Then the correction due to $d\gamma^z/dh$ in Eq. (28) is already of order $1/M$, and therefore only terms to leading order in $1/M$, arising from the transverse spin fluctuations can be retained when calculating the derivative. To calculate $d\gamma^z(\mathbf{k},\mathbf{k};i\nu_n,i\nu_n)/dh$ we differentiate the equation for the self-energy (25) twice with respect to the field. Note that the terms containing $d^2\gamma^\pm/dh^2$ should be retained in this calculation, since they are not small in $1/M$ and do not vanish in the $q \to 0$ limit contrary to $d\gamma^\pm/dh$. After lengthy algebraic manipulations we finally obtain

$$\left[\frac{d}{dh}\gamma^z(\mathbf{k},\mathbf{k};i\nu_n,i\nu_n) \right]_{h=0} = 2[1+U\chi(\mathbf{0},0)]$$
$$\times \frac{T}{N} \sum_{\mathbf{q},i\omega_n} \gamma^3(\mathbf{k},\mathbf{k}+\mathbf{q};i\nu_n,i\nu_n+i\omega_n)$$
$$\times G^3(\mathbf{k}+\mathbf{q},i\omega_n+i\nu_n)\chi^{+-}(\mathbf{q},i\omega_n)$$
$$+ O(1/M).$$

$$(29)$$

Generally, the susceptibilities (24) which enter Eqs. (25) and (27) can be represented in a form similar to Eq. (11) or (12) at $\omega=0$,

$$\chi^{+-}(\mathbf{q},0) = 2\chi^{zz}(\mathbf{q},0) \simeq \frac{R}{q^2+\xi^{-2}} + \text{regular terms}, \quad (30)$$

where R is a constant. As in localized-moment systems with strong short-range order,[48] the following identity:

$$\langle \mathbf{S}_0 \cdot \mathbf{S_r} \rangle \simeq \frac{T}{N} \sum_{\mathbf{q}} \left[\chi^{zz}(\mathbf{q},0) + \frac{M-1}{2}\chi^{+-}(\mathbf{q},0) \right] e^{i\mathbf{q}\cdot\mathbf{r}}$$
$$= \overline{S_0^2} \exp(-r/\xi), \quad (31)$$

which incorporates the correct long distance asymptotics of the real-space correlation functions at $T \ll T^*$, is useful to relate R and $\overline{S_0}$. As a result, we obtain

$$\overline{S_0^2} = \frac{M}{4\pi} TR \ln \xi. \quad (32)$$

Since the dominant contribution to momentum sums in Eqs. (25) and (27) arises from the long wavelength region $q \lesssim \xi^{-1}$, we replace

$$\gamma_{\sigma,\sigma'}^a(\mathbf{k},\mathbf{k}+\mathbf{q};i\nu_n,i\nu_n) \to \gamma_{\sigma,\sigma'}^a(\mathbf{k},\mathbf{k};i\nu_n,i\nu_n),$$
$$\frac{d}{dh}\gamma^z(\mathbf{k},\mathbf{k}+\mathbf{q};i\nu_n,i\nu_n+i\omega_n) \to \frac{d}{dh}\gamma^z(\mathbf{k},\mathbf{k};i\nu_n,i\nu_n).$$

$$(33)$$

Equations (25), (27), and (29) together with the replacements (33) form a closed system for γ and Σ. The remaining integrals over q are easily calculated analytically analogous to the non-self-consistent calculation in Sec. II A. After the continuation to the real axis we obtain the following algebraic equations for the self-energy and the irreducible vertex γ for $t\xi^{-1} \ll |\omega-\varepsilon_{\mathbf{k}}| \ll t$:

$$\Sigma(\mathbf{k},\omega) = \frac{\Delta_0^2 \gamma(\mathbf{k},\mathbf{k};\omega,\omega)}{\omega - \varepsilon_{\mathbf{k}} - \Sigma(\mathbf{k},\omega)},$$

$$\gamma(\mathbf{k},\mathbf{k};\omega,\omega) = 1 - \frac{M-2}{M}\frac{\Delta_0^2 \gamma^2(\mathbf{k},\mathbf{k};\omega,\omega)}{[\omega-\varepsilon_{\mathbf{k}}-\Sigma(\mathbf{k},\omega)]^2}$$
$$+ \frac{2}{M}\frac{\Delta_0^4 \gamma^3(\mathbf{k},\mathbf{k};\omega,\omega)}{[\omega-\varepsilon_{\mathbf{k}}-\Sigma(\mathbf{k},\omega)]^4}, \quad (34)$$

where we have introduced the ground state spin splitting $\Delta_0 = U\overline{S_0}$. Similar to the TPSC approach of Sec. II A, the resulting self-energy and the vertex depend on $\mathbf{k}$ only through $\overline{\omega} = \omega - \varepsilon_{\mathbf{k}}$ and are given by

$$\Sigma(\mathbf{k},\omega) = \frac{M(\Delta_0^2 + \overline{\omega}^2 - \sqrt{\overline{\omega}^2-\alpha_1\Delta_0^2}\sqrt{\overline{\omega}^2-\alpha_2\Delta_0^2})}{2(2+M)\overline{\omega}},$$

$$\gamma(\mathbf{k},\mathbf{k};\omega,\omega) = \frac{M}{2(2+M)^2\Delta_0^2\overline{\omega}^2}[2\overline{\omega}^4 + (6+M)\Delta_0^2\overline{\omega}^2 - M\Delta_0^4$$
$$+ (M\Delta_0^2 - 2\overline{\omega}^2)\sqrt{\overline{\omega}^2-\alpha_1\Delta_0^2}\sqrt{\overline{\omega}^2-\alpha_2\Delta_0^2}],$$

$$(35)$$

where $\alpha_{1,2} = 1+4(1\pm\sqrt{1+M/2})/M$; the branch $\text{Im}\sqrt{z} \geq 0$ of the square roots is chosen to guarantee the correct analytical properties for Σ and γ. On the other hand, in the absence of the vertex renormalization, i.e., for $\gamma(\mathbf{k},\mathbf{k};i\nu_n,i\nu_n)=1$, which is the analog of the FLEX approximation[49] in our approach, we obtain for the self-energy the M-independent result
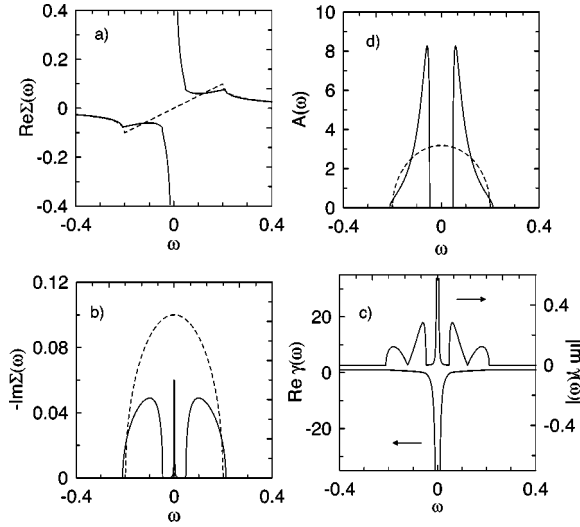
FIG. 6. The real and imaginary parts of the self-energy (a), (b), the spectral function (c), and the vertex function γ (d) at $T \ll T^*$ in the fully self-consistent Ward identity approach (solid lines) and the FLEX-like approach, which is self-consistent with respect to the self-energy only (dashed lines) as a function of $\bar{\omega} = \omega - \varepsilon_{\mathbf{k}}$ at $\Delta_0 = 0.1$.

$$\Sigma(\mathbf{k}, \omega) = \frac{1}{2}(\bar{\omega} - \sqrt{\bar{\omega} - 2\Delta_0}\sqrt{\bar{\omega} + 2\Delta_0}). \qquad (36)$$

To zeroth order in $1/M$ (i.e., at $M = \infty$) we obtain from Eq. (35)

$$\Sigma(\mathbf{k}, \omega) = \frac{\Delta_0^2}{\bar{\omega}}, \quad \gamma(\mathbf{k}, \mathbf{k}; \omega, \omega) = 1 - \frac{\Delta_0^2}{\omega^2}, \qquad (37)$$

i.e., the self-energy and the vertex corrections exactly cancel each other at $M = \infty$ and the self-energy and the vertex are given by their second-order, non-self-consistent results. To demonstrate how this result changes at finite values of M, we plot in Fig. 6 the results (35) and (36) for $M = 3$ together with the corresponding spectral functions. Similarly to the non-self-consistent solution (37) the real part of the self-energy in the self-consistent solution (35) is divergent at $\omega = 0$. This is in contrast to the solution (36), which is self-consistent with respect to the self-energy only, and leads to a finite positive slope of the real part of the self-energy at the Fermi level $\partial \text{Re}\Sigma / \partial \omega = 1/2$. The imaginary part of the self-energy has its largest absolute value at the Fermi energy and monotonically decreases with $|\omega|$ for the solution (36), while it has more complicated energy dependence with a δ-function singularity at $\omega = 0$ according to the self-consistent result (35). As a consequence, the solution (36), which is self-consistent with respect to the self-energy only, displays a one-peak structure of the spectral function, while Eq. (35) leads to a two-peak structure of the spectral function [Fig. 6(c)], which is similar to the $M = \infty$ result (37). We note that the gap in the spectral function at the Fermi energy in the self-consistent solution is most likely an artifact of the first order in $1/M$ result. At the same time the similarities between the results in zeroth and first order in $1/M$ allow to conclude that the higher order

corrections in $1/M$ are expected to be small and do not lead to qualitative changes.

The one-peak structure of the spectral functions in the solution without vertex renormalization is similar to that in the FLEX approximation in the AFM case, which predicts only a slight variation of the quasiparticle weight around the Fermi surface.[7] As discussed in Ref. 9, this result is a drawback of the absence of vertex corrections, and the necessity to account for frequency-dependent vertex renormalization *together* with the self-energy corrections is crucial in this case. As we have shown in this section, a similar conclusion is reached in the FM case; the corresponding nontrivial frequency dependence of the vertex is shown in Fig. 6(d).

Therefore, the solution (35) which accounts for both self-energy and vertex corrections leads to the results which are qualitatively similar to those obtained in non-self-consistent approaches of Sec. II. The same arguments can be applied to the s-d model, which is therefore expected to lead to the similar results at $T \ll T^*$.

IV. SUMMARY AND CONCLUSION

We have investigated the self-energy in two dimensions in the vicinity of a FM instability within the TPSC, the one-loop fRG analysis, and by applying Ward identities. In all approaches the self-energy has a non-Fermi-liquid form in narrow window $|\omega| \lesssim \Delta_0$ around the Fermi level, and the spectral functions have a two-peak structure at low temperatures. The spectral weight at the Fermi energy is strongly suppressed at $T \lesssim T^*$ in both, non-self-consistent and self-consistent solutions, because the self-energy and the vertex corrections partially cancel each other. The form of the spectral functions we have obtained in the paramagnetic (PM) state with strong short-range magnetic order is qualitatively similar to the mean-field result for the spectral functions in the FM ordered state, if the electron spin quantization axis is chosen *perpendicular* to the direction of the magnetization. Indeed, performing the simplest Stoner-like decoupling of the interaction in the Hubbard model with the order parameter $\Delta = (U/2)\langle c_{i\uparrow}^\dagger c_{i\downarrow} + c_{i\downarrow}^\dagger c_{i\uparrow} \rangle$, which corresponds to a spin alignment along the x axis, we readily obtain

$$\langle\langle c_{\mathbf{k}\sigma}^\dagger | c_{\mathbf{k}\sigma} \rangle\rangle_\omega = \frac{1}{2}\left(\frac{1}{\omega - \varepsilon_{\mathbf{k}} - \Delta + i0^+} + \frac{1}{\omega - \varepsilon_{\mathbf{k}} + \Delta + i0^+}\right), \qquad (38)$$

where $\langle\langle | \rangle\rangle_\omega$ denotes the Fourier transform of the retarded Green function. With the inclusion of a small damping $i\gamma$ in the denominators the Green function Eq. (38) leads indeed to a spectral function, which is qualitatively similar to, e.g., Fig. 6(c). At the same time, the mean-field Green functions for the spin projection *along* (parallel or antiparallel) the magnetization axis are given by

$$\frac{1}{2}\langle\langle c_{\mathbf{k}\uparrow}^\dagger \pm c_{\mathbf{k}\downarrow}^\dagger | c_{\mathbf{k}\uparrow} \pm c_{\mathbf{k}\downarrow} \rangle\rangle_\omega = \frac{1}{\omega - \varepsilon_{\mathbf{k}} \mp \Delta + i0^+} \qquad (39)$$

and are qualitatively different from the result of Eq. (38). The spectral functions in the PM phase are necessarily spin-rotation invariant. Therefore, we expect strong changes of
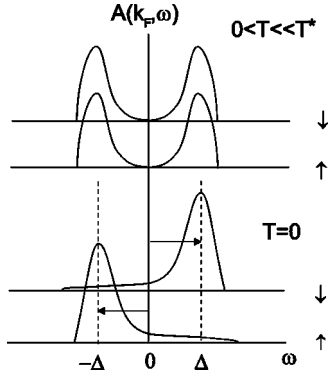
FIG. 7. Schematic picture for the evolution of the spectral function near the ferromagnetic phase transition. The spectral functions at $T=0$ are shown at the paramagnetic Fermi surface. The spectral functions at the Fermi surfaces of spin-up and spin-down electrons are expected to shift by $\pm\Delta$ with respect to those of the paramagnetic Fermi surface, as indicated by arrows.

the spectral functions at the zero temperature FM phase transition only for a choice of the spin quantization axis along the direction of the ground-state magnetization **M**, while spectral functions for electrons with spin quantization axis perpendicular to **M** change continuously with decreasing the temperature to zero (or to the Curie temperature $T_C \ll t$ for quasi-2D systems). Note also that beyond the mean-field approximation, the Green functions for a spin projection antiparallel to **M** acquire strong incoherent contributions, at least for fully polarized ferromagnets.[14,15] The overall qualitative picture for the evolution of the spectral properties summarizes parts of the results of the present paper in Fig. 7.

The two-peak structure of the spectral functions in the vicinity of a FM instability leads to the formation of new coherent quasiparticles at the points of the Brillouin zone near the spin-up and spin-down Fermi surfaces of the FM ordered ground state. The spin-rotation symmetry remains, however, necessarily unbroken at $T>0$ and new "preformed" qp's do not have any preferable spin direction. This "uncertainty" of the spin direction in 2D magnets with strong short-range order was earlier discussed in connection with NMR technique, which is expected to give two-peak NMR spectra,[50] even in arbitrary small static magnetic field. For quasi-two-dimensional systems the quasisplitting of the Fermi surface is expected at $T_C < T \ll \Delta_0$ with Δ_0 being the ground-state spin splitting.

Translated to real space, "domains" of size $\sim\xi$ may form containing mostly electrons with a certain spin polarization. Unlike in localized-moments systems, however, these "domains" have a small electronic density and are therefore expected to be not a static but rather a dynamic phenomenon. Such a dynamic formation of droplets with a preferred spin direction near the FM instability should be distinguished from the possible phase separation into hole-rich and hole-poor regions[51–54] in the vicinity of an AFM instability for the almost half-filled band. The latter may result as a compromise to "adjust" an AFM spin structure to an electron density $n<1$ and involve charge fluctuations which are coupled to the spin channel for a nearly half-filled band. At the same time, the dynamic domain formation near a FM instability is expected solely due to FM spin fluctuations which favor the aggregation of electrons with certain spin orientation in regions of size $\sim\xi$.

While the form of the spectral functions in the vicinity of the FM phase transition is dramatically different from the conventional quasiparticle one-peak structure, we do not expect sizable effects in the density of states. Indeed, since the spectral functions depend at low energy on $\varepsilon - \varepsilon_{\mathbf{k}}$ only, we find for $|\varepsilon| \ll t$

$$\rho(\varepsilon) = \frac{1}{N}\sum_{\mathbf{k}} A(\mathbf{k},\varepsilon) \simeq \int_{\varepsilon_{\min}}^{\varepsilon_{\max}} d\varepsilon' \rho_0(\varepsilon') A(\varepsilon - \varepsilon'), \quad (40)$$

where $\rho_0(\varepsilon)$ is the bare density of states and $\varepsilon_{\min,\max}$ are the energies of the bottom and the top of the band with respect to the Fermi level. Taking into account the two-peak structure of $A(\varepsilon)$ we obtain

$$\rho(\varepsilon) \simeq \frac{1}{2}[\rho_0(\varepsilon - \Delta) + \rho_0(\varepsilon + \Delta)], \quad (41)$$

i.e., the density of states is also "presplit" at low T, but is not strongly suppressed at the Fermi level.

Our results may provide the possibility to interpret angle-resolved photoemission spectroscopy (ARPES) data of layered ferromagnetic materials. For example, the described effects may be important in the interpretation of the results of ARPES studies of the layered manganite compound $La_{1+x}Sr_{2-x}Mn_2O_7$.[3] Pseudogap structures are observed in this material both, above and below T_C. It was suggested that these structures are possibly produced by an accompanying charge order,[55] or by phase separation.[56] The FM fluctuations, however, might be responsible for part of the pronounced shift ($\sim$250 meV) of the spectral weight maxima away from the Fermi energy at the points of the Brillouin zone near the FM Fermi surface with T above the Curie temperature T_C.

The described effects may be also important for the normal state of some unconventional superconductors, where ferromagnetic fluctuations are expected to be important (see UGe_2, Sr_2RuO_4). UGe_2 has long-range magnetic order in the ground state and therefore may also show a quasisplitting of the FS above T_C. Although long range FM order is absent in strontium ruthenate Sr_2RuO_4, FM order is induced by a small amount of La doping.[57]

Taking into account the strong self-energy and vertex corrections in the vicinity of the FM phase transition, the criteria for ferromagnetism[18] should be reconsidered. This especially concerns quasi-2D systems, where these renormalizations are expected to be the strongest. However, even in 3D systems, where the finite-temperature divergencies of the self-energy at the Fermi level are only logarithmic in ξ (instead of a power law divergence in 2D), they can also lead to additional renormalizations of the Stoner criterion in comparison to those considered within the paramagnon (spin fluctuation) theory of Refs. 18 and 19.

So far unresolved is the behavior of the self-energy in the quantum-critical regime, if it exists at all for the FM phase transition due to the presence of nonanalytic contributions.

This behavior depends crucially on the temperature dependence of the correlation length; the $\varepsilon^{2/3}$ dependence of the self-energy at $T=0$, however, already implies a nontrivial temperature dependence of the quasiparticle scattering rate at finite temperatures. The simple ansatz for the magnetic susceptibility we have used in the Ward identity approach is not justified in this case, and an alternative approach has yet to be developed.

[1] A. Damascelli, Z. Hussain, and Z.-X. Shen, Rev. Mod. Phys. **75**, 473 (2003).

[2] S.-C. Wang, H.-B. Yang, A. K. P. Sekharan, H. Ding, J. R. Engelbrecht, X. Dai, Z. Wang, A. Kaminski, T. Valla, T. Kidd, A. V. Fedorov, and P. D. Johnson, Phys. Rev. Lett. **92**, 137002 (2004).

[3] D. S. Dessau, T. Saitoh, C.-H. Park, Z.-X. Shen, P. Villella, N. Hamada, Y. Moritomo, and Y. Tokura, Phys. Rev. Lett. **81**, 192 (1998); T. Saitoh, D. S. Dessau, Y. Moritomo, T. Kimura, Y. Tokura, and N. Hamada, Phys. Rev. B **62**, 1039 (2000).

[4] A. P. Kampf and J. R. Schrieffer, Phys. Rev. B **41**, 6399 (1990); **42**, 7967 (1990).

[5] J. Schmalian, D. Pines, and B. Stojkovic, Phys. Rev. Lett. **80**, 3839 (1998); Phys. Rev. B **60**, 667 (1999); A. V. Chubukov and J. Schmalian, *ibid.* **57**, R11 085 (1998).

[6] Ar. Abanov, A. V. Chubukov, and J. Schmalian, Adv. Phys. **52**, 119 (2003).

[7] J. J. Deisz, D. W. Hess, and J. W. Serene, Phys. Rev. Lett. **76**, 1312 (1996).

[8] J. Altmann, W. Brenig, and A. P. Kampf, Eur. Phys. J. B **18**, 429 (2000).

[9] J. Vilk and A.-M. S. Tremblay, J. Phys. I **7**, 1309 (1997); B. Kyung, Phys. Rev. B **58**, 16 032 (1998); S. Moukouri, S. Allen, F. Lemay, B. Kyung, D. Poulin, Y. M. Vilk, and A.-M. S. Tremblay, *ibid.* **61**, 7887 (2000).

[10] C. Huscroft, M. Jarrell, Th. Maier, S. Moukouri, and A. N. Tahvildarzadeh, Phys. Rev. Lett. **86**, 139 (2001).

[11] A. A. Katanin and A. P. Kampf, Phys. Rev. Lett. **93**, 106406 (2004).

[12] D. Rohe and W. Metzner, cond-mat/0406164 (unpublished).

[13] V. Yu. Irkhin and M. I. Katsnelson, Phys. Rev. B **62**, 5647 (2000).

[14] J. A. Hertz and D. M. Edwards, J. Phys. F: Met. Phys. **3**, 2174 (1973); **3**, 2191 (1973).

[15] V. Yu. Irkhin and M. I. Katsnelson, J. Phys.: Condens. Matter **2**, 7151 (1990); Usp. Fiz. Nauk **164**, 705 (1994) [Phys. Usp. **37**, 659 (1994)].

[16] W. F. Brinkman and S. Engelsberg, Phys. Rev. **169**, 417 (1968).

[17] I. E. Dzyaloshinskii and P. S. Kondratenko, Sov. Phys. JETP **43**, 1036 (1976).

[18] T. Moriya, *Spin Fluctuations in Itinerant Electron Magnetism* (Springer, Berlin, 1985).

[19] P. C. E. Stamp, J. Phys. F: Met. Phys. **15**, 1829 (1985).

[20] S. Doniach and S. Engelsberg, Phys. Rev. Lett. **17**, 750 (1966).

[21] N. Nagaosa and P. A. Lee, Phys. Rev. Lett. **64**, 2450 (1990); P. A. Lee and N. Nagaosa, Phys. Rev. B **46**, 5621 (1992).

[22] C. Castellani, C. Di Castro, and M. Grilli, Phys. Rev. Lett. **75**, 4650 (1995); C. Castellani, S. Caprara, C. Di Castro, and A. Maccarone, Nucl. Phys. B **594**, 747 (2001).

[23] W. Metzner, D. Rohe, and S. Andergassen, Phys. Rev. Lett. **91**, 066402 (2003).

[24] B. L. Altshuler, L. B. Ioffe, and A. J. Millis, Phys. Rev. B **50**, 14 048 (1994).

[25] S. Sachdev, *Quantum Phase Transitions* (Cambridge University Press, Cambridge, 1999).

[26] V. Hankevych, B. Kyung, and A.-M. S. Tremblay, Phys. Rev. B **68**, 214405 (2003).

[27] P. Monthoux, Phys. Rev. B **68**, 064408 (2003).

[28] D. Belitz, T. R. Kirkpatrick, and T. Vojta, Phys. Rev. B **55**, 9452 (1997); A. V. Chubukov and D. L. Maslov, *ibid.* **68**, 155113 (2003); A. V. Chubukov, C. Pepin, and J. Rech, Phys. Rev. Lett. **92**, 147003 (2004).

[29] D. Zanchi and H. J. Schulz, Phys. Rev. B **54**, 9509 (1996); **61**, 13 609 (2000).

[30] C. J. Halboth and W. Metzner, Phys. Rev. B **61**, 7364 (2000); Phys. Rev. Lett. **85**, 5162 (2000).

[31] C. Honerkamp, M. Salmhofer, N. Furukawa, and T. M. Rice, Phys. Rev. B **63**, 035109 (2001); M. Salmhofer and C. Honerkamp, Prog. Theor. Phys. **105**, 1 (2001).

[32] C. Honerkamp and M. Salmhofer, Phys. Rev. Lett. **87**, 187004 (2001); Phys. Rev. B **64**, 184516 (2001).

[33] A. A. Abrikosov, Physics (Long Island City, N.Y.) **2**, 5 (1965); Yu. A. Bychkov, L. P. Gor'kov, and I. E. Dzyaloshinskii, Zh. Eksp. Teor. Fiz. **50**, 738 (1966) [Sov. Phys. JETP **23**, 489 (1966)].

[34] N. E. Bickers and S. R. White, Phys. Rev. B **43**, 8044 (1991).

[35] V. Janis, J. Phys.: Condens. Matter **10**, 2915 (1998).

[36] S. V. Vonsovskij, *Magnetism* (New York, 1974).

[37] E. L. Nagaev, *Physics of Magnetic Semiconductors* (Mir, Moscow, 1983); Phys. Rep. **346**, 387 (2001).

[38] A. A. Katanin and A. P. Kampf, Phys. Rev. B **68**, 195101 (2003).

[39] P. Kopietz and S. Chakravarty, Phys. Rev. B **40**, 4858 (1989).

[40] J. Gonzalez, F. Guinea, and M. A. H. Vozmediano, Nucl. Phys. B **485**, 694 (1997).

[41] A. V. Chubukov, S. Sachdev, and J. Ye, Phys. Rev. B **49**, 11 919 (1994).

[42] V. Yu. Irkhin, A. A. Katanin, and M. I. Katsnelson, Phys. Rev. Lett. **89**, 076401 (2002).

[43] C. Honerkamp, Eur. Phys. J. B **21**, 81 (2001); C. Honerkamp and M. Salmhofer, Phys. Rev. B **67**, 174504 (2003).

[44] H. J. Vidberg and J. W. Serene, J. Low Temp. Phys. **29**, 179 (1977).

[45] P. Bloom, Phys. Rev. B **12**, 125 (1975).

[46] W. Metzner, C. Castellani, and C. di Castro, Adv. Phys. **47**, 317 (1998).

[47] V. Yu. Irkhin and A. A. Katanin, Phys. Rev. B **55**, 12 318 (1997).

[48] V. Yu. Irkhin and M. I. Katsnelson, J. Phys.: Condens. Matter **3**, 6439 (1991).

[49] N. E. Bickers, D. J. Scalapino, and S. R. White, Phys. Rev. Lett. **62**, 961 (1989); N. E. Bickers and D. J. Scalapino, Ann. Phys. (N.Y.) **193**, 206 (1989).

[50] V. Yu. Irkhin and M. I. Katsnelson, Z. Phys. B: Condens. Matter **62**, 201 (1986); Eur. Phys. J. B **19**, 401 (2001).

[51] P. B. Visscher, Phys. Rev. B **10**, 932 (1974); **10**, 943 (1974).

[52] E. L. Nagaev, Usp. Fiz. Nauk **165**, 529 (1995) [Phys. Usp. **38**, 497 (1995)].

[53] E. Dagotto, and J. Riera, Phys. Rev. B **46**, 12084 (1992); E. Dagotto, J. Riera, Y. C. Chen, A. Moreo, A. Nazarenko, F. Alcaraz, and F. Ortolani, *ibid.* **49**, 3548 (1994).

[54] W. O. Putikka and M. U. Luchini, Phys. Rev. B **62**, 1684 (2000).

[55] H. Aliaga, D. Magnoux, A. Moreo, D. Poilblanc, S. Yunoki, and E. Dagotto, Phys. Rev. B **68**, 104405 (2003).

[56] A. Moreo, S. Yunoki, and E. Dagotto, Phys. Rev. Lett. **83**, 2773 (1999).

[57] N. Kikugawa, C. Bergemann, A. P. Mackenzie, and Y. Maeno, cond-mat/0211248 (unpublished); N. Kikugawa, A. P. Mackenzie, C. Bergemann, R. A. Borzi, S. A. Grigera and Y. Maeno, Phys. Rev. B **70**, 060508 (2004).